EUROPEAN ORGANISATION FOR NUCLEAR RESEARCH

CERN-PPE/95-42
3 April 1995

# One-prong $\tau$ Decays with Neutral Kaons

The L3 Collaboration

## Abstract

We have analyzed one-prong $\tau$ decays with neutral kaons using the information from a fine-grained hadron calorimeter. The data sample consists of 43 500 $\mathrm{Z} \rightarrow \tau^{+}\tau^{-}(\gamma)$ events collected by the L3 detector at LEP in 1991, 1992 and 1993. The following branching fractions are measured: $\mathcal{B}(\tau^{-} \rightarrow \nu_{\tau}\pi^{-}\bar{\mathrm{K}}^{0}) = 0.0095 \pm 0.0015(\mathrm{stat}) \pm 0.0006(\mathrm{syst})$; $\mathcal{B}(\tau^{-} \rightarrow \nu_{\tau}\pi^{-}\pi^{0}\bar{\mathrm{K}}^{0}) = 0.0041 \pm 0.0012(\mathrm{stat}) \pm 0.0003(\mathrm{syst})$ and $\mathcal{B}(\tau^{-} \rightarrow \nu_{\tau}\pi^{-}\mathrm{K}^{0}\bar{\mathrm{K}}^{0}) = 0.0031 \pm 0.0012(\mathrm{stat}) \pm 0.0004(\mathrm{syst})$.

Submitted to *Phys. Lett. B*

# Introduction

Measurements of the branching fractions of $\tau$-lepton decays with neutral kaons are important for understanding $\tau$ decays [1], in particular the compatibility of inclusive and exclusive branching fractions. They also provide new information on the dynamics of neutral kaon production which is not yet well understood. Many factors affect the calculation of the branching fractions for these decays, such as Cabibbo-suppression for modes with odd numbers of kaons, very limited phase space for the modes with two kaons, QCD anomalies and uncertainties in the resonant structure. Their interplay prevents firm theoretical predictions from being made [2,3].

In this paper we present an analysis of the following decay modes: $\tau^- \to \nu_\tau \pi^- \bar{\mathrm{K}}^0$, $\tau^- \to \nu_\tau \pi^- \pi^0 \bar{\mathrm{K}}^0$, and $\tau^- \to \nu_\tau \pi^- \mathrm{K}^0 \bar{\mathrm{K}}^0$, where the charge conjugate decays are also implied here and throughout this paper. The fine-grained hadron calorimeter of L3 is used to detect neutral kaons and to measure their energies and directions. The selection of $\tau$ decays with neutral kaons is based on the coincidence of high energy deposition in the hadron calorimeter and a low momentum charged track detected in the central tracker. The L3 detector is well suited to this measurement as the efficiencies for detecting the $\mathrm{K_L}$ and $\mathrm{K_S}$ components of $\mathrm{K}^0$ are comparable due to the small decay volume.

The data sample used in this analysis corresponds to an integrated luminosity of 69pb$^{-1}$ collected at $\sqrt{s} \approx M_\mathrm{Z}$ during the 1991, 1992 and 1993 LEP running periods.

# The L3 Detector

The L3 detector is described in detail in reference 4. The $\mathrm{e^+e^-}$ collision point is surrounded by a tracking chamber, a high resolution electromagnetic calorimeter, a cylindrical shell of scintillation counters, a hadron calorimeter, and a muon chamber system. The detector is installed in a large magnet providing a uniform 0.5 Tesla field.

The hadron calorimeter (HCAL) is the key subdetector for this measurement. It covers the polar angle range $5^\circ < \theta < 175^\circ$ and consists of depleted uranium absorber plates interleaved with proportional wire chambers oriented alternately parallel and perpendicular to the beam direction. The readout, which is grouped into cells in both of these projections as well as in depth, provides a three dimensional pattern for hadronic showers. The energy resolution of the calorimeter for $\pi^\pm$ is determined to be $55\%/\sqrt{E(\mathrm{GeV})} + 8\%$ in the central region. The angular resolution is better than 40 mrad in both the polar and azimuthal projections for hadronic showers above 6 GeV, which is approximately the minimum energy of $\mathrm{K}^0$'s from $\tau$ decays at LEP. The detailed study of the hadron calorimeter prototype is described elsewhere [5].

The electromagnetic calorimeter (ECAL) is composed of bismuth germanate crystals in the shape of truncated pyramids pointing to the interaction region. The ECAL barrel has a polar angle coverage of $42^\circ < \theta < 138^\circ$, while the end-caps cover the regions $12^\circ < \theta < 38^\circ$ and $142^\circ < \theta < 168^\circ$.

The central tracking detector consists of a time expansion chamber (TEC) with high spatial resolution in the plane normal to the beam direction. TEC is surrounded by a Z-chamber which supplements the $r - \phi$ measurement with a $z$-coordinate measurement. The transverse momentum resolution of the tracking chamber is $\sigma(1/P_\mathrm{T}) = 0.018\ (\mathrm{GeV/c})^{-1}$ in the central region ($|\cos\theta_{TEC}| < 0.7$). The position resolution of a track extrapolated to the calorimeters is 0.2 mm in the plane transverse to the beam direction and 1.5 mm along the beam axis.

## Selection of $Z \rightarrow \tau^+\tau^-(\gamma)$ Events

The selection of $\tau$ decays is done independently in two hemispheres separated by the plane perpendicular to the thrust axis of the event. Particle identification in each hemisphere is based upon the topological properties of the energy deposition in the electromagnetic and hadron calorimeters with respect to the trajectory of the charged track.

The selection of $\tau$ decays proceeds in three steps. First, a sample of low multiplicity, back-to-back events is selected, consisting mainly of leptons from Z decays. This preselection suppresses such backgrounds as hadronic Z decays, two-photon interactions, cosmic muons, and beam-gas interactions. In the second step, the individual $\tau$ decays are identified. Finally, requirements are placed on the hemisphere opposite to the identified $\tau$ decay candidate in order to suppress the remaining non-$\tau$ background. The selection procedure is described in detail in reference 6. A sample of 45 262 events is selected in the fiducial volume $46° < \theta < 134°$.

The selection efficiency for $Z \rightarrow \tau^+\tau^-(\gamma)$ events is calculated to be 57.8% using the KORALZ Monte Carlo program [7,8] with a full simulation of the L3 detector response [1]. The main source of inefficiency is the geometric acceptance. The $Z \rightarrow \tau^+\tau^-(\gamma)$ Monte Carlo sample contains 674 000 generated events, which corresponds to nine times more $Z \rightarrow \tau^+\tau^-(\gamma)$ events than in the data sample. The background contamination from non-$\tau$ sources includes 1.9% of $e^+e^-(\gamma)$, 1.0% of $\mu^+\mu^-(\gamma)$, 0.4% of $Z \rightarrow$ hadrons events, 0.4% of two-photon reactions, and 0.2% of cosmic muon events and beam-gas interactions. These estimates are derived primarily from the data using either the side opposite to the selected decay or global event characteristics. The corresponding Monte Carlo simulation for the background [7, 11] is used only to verify these estimates. The total number of $Z \rightarrow \tau^+\tau^-(\gamma)$ events in the sample is estimated to be 43 497$\pm$60, where the error includes the uncertainty in the background evaluation.

## Selection of $\tau$ Decays with Neutral Kaons

To select a $\tau^- \rightarrow \nu_\tau K^0 X^-$ candidate [2], exactly one track is required in the hemisphere. This track must be consistent with originating from the interaction point in the plane perpendicular to the beam direction. The expected energy deposition of the track in the HCAL is estimated from its momentum in the TEC and energy in the ECAL associated to it using the reconstruction technique described in reference 6. Any HCAL energy deposition exceeding this estimate, $\Delta E_{\mathrm{HC}} = E_{\mathrm{HC}}^{\mathrm{tot}} - E_{\mathrm{HC}}^{\pi^-} > 0$, could be due to a fluctuation in the charged hadron shower, which is approximately proportional to $\sqrt{P_\pi}$, or due to the presence of neutral kaons. In order to suppress fluctuations, the ratio $\Delta E_{\mathrm{HC}}/\sqrt{P_\pi}$ must be greater than 5 $(\mathrm{GeV})^{1/2}$ (Figure 1a). This cut rejects a large fraction of $\tau$ decays with no $K^0$ and almost all residual background from non-$\tau$ sources. No $\tau$ decays with the charged particle momentum greater than 15 GeV/c survive this cut.

The dominant backgrounds after the previous cut are $\tau^- \rightarrow \rho^-\nu_\tau$ and $\tau^- \rightarrow a_1^-\nu_\tau$ decays with $\pi^0$ leakage from the ECAL to the HCAL. This background is suppressed by requiring the energy in the first three HCAL layers ($18X_0$) to be less than 80% of the total energy deposition in the HCAL (Figure 1b). The angular separation between the $\pi^-$ and $K^0$, $\alpha_{\pi-K^0}$, is estimated as the difference between the center of gravity of the HCAL cluster and impact position of the

[1] The L3 detector simulation is based on GEANT Version 3.14; see ref. [9]. The GHEISHA program [10] is used to simulate hadronic interactions.

[2] The hadronic system $X^-$ contains a single charged hadron and any number of neutral hadrons.

track in the HCAL. It is required to be $0.03 < \alpha_{\pi-\mathrm{K}^0} < 0.2$ rad (Figure 1c). This cut improves the purity of the selected sample.

After applying these selection criteria, 247 $\tau^- \to \nu_\tau \mathrm{K}^0 \mathrm{X}^-$ candidate decays remain with 27.7 decays expected from the modes without $\mathrm{K}^0$'s. The following $\tau$ decays contribute to the signal: $\tau^- \to \nu_\tau \pi^- \bar{\mathrm{K}}^0$, $\tau^- \to \nu_\tau \mathrm{K}^- \mathrm{K}^0$, $\tau^- \to \nu_\tau \pi^- \pi^0 \bar{\mathrm{K}}^0$, $\tau^- \to \nu_\tau \mathrm{K}^- \pi^0 \mathrm{K}^0$, and $\tau^- \to \nu_\tau \pi^- \mathrm{K}^0 \bar{\mathrm{K}}^0$. The efficiencies are estimated to be 13.0%, 5.3%, 8.8%, 3.7% and 19.8% in the fiducial volume respectively. The composition of the selected sample of $\mathrm{K}^0$'s corresponds to 68% $\mathrm{K}^0_\mathrm{L}$ and 32% $\mathrm{K}^0_\mathrm{S}$. The modes $\tau^- \to \nu_\tau \mathrm{K}^- \mathrm{K}^0$ and $\tau^- \to \nu_\tau \mathrm{K}^- \pi^0 \mathrm{K}^0$ have significantly lower efficiency than the corresponding modes with charged pions due to less advantageous energy sharing between $\mathrm{K}^- \mathrm{K}^0$ in the laboratory frame compared to $\pi^- \bar{\mathrm{K}}^0$ [3].

# Determination of the Branching Fractions

In order to distinguish $\tau^- \to \nu_\tau \pi^- \bar{\mathrm{K}}^0$ decays from $\tau^- \to \nu_\tau \pi^- \pi^0 \bar{\mathrm{K}}^0$ and $\tau^- \to \nu_\tau \pi^- \mathrm{K}^0 \bar{\mathrm{K}}^0$ decays, the selected decays are classified into three categories:

1. Decays with a $\pi^0$ candidate ($\tau^- \to \nu_\tau \pi^- \pi^0 \bar{\mathrm{K}}^0$ candidates).
   These decays are required to have an energy cluster in the ECAL of greater than 6 GeV and a transverse shower shape consistent with a $\pi^0$. A typical candidate is shown in Figure 2.

2. Decays with extra neutral hadronic energy ($\tau^- \to \nu_\tau \pi^- \mathrm{K}^0 \bar{\mathrm{K}}^0$ candidates).
   Two high energy hadronic showers from a $\mathrm{K}^0 \bar{\mathrm{K}}^0$ pair are not separated in angle but are often separated in depth (Figure 3). Therefore, they are characterized by a more uniform energy deposition than a single neutral hadronic shower. In order to select these decays, the energy deposition in the ECAL, and in the front and back parts of the HCAL are each required to exceed 10% of the total energy associated to neutral kaons.

3. Remaining decays ($\tau^- \to \nu_\tau \pi^- \bar{\mathrm{K}}^0$ candidates).

For each category, the total number of decays is a linear combination of the signal channels: $\tau^- \to \nu_\tau \pi^- \bar{\mathrm{K}}^0$, $\tau^- \to \nu_\tau \mathrm{K}^- \mathrm{K}^0$, $\tau^- \to \nu_\tau \pi^- \pi^0 \bar{\mathrm{K}}^0$, $\tau^- \to \nu_\tau \mathrm{K}^- \pi^0 \mathrm{K}^0$, and $\tau^- \to \nu_\tau \pi^- \mathrm{K}^0 \bar{\mathrm{K}}^0$ and the background channels. Only the coefficients for the modes $\tau^- \to \nu_\tau \pi^- \bar{\mathrm{K}}^0$, $\tau^- \to \nu_\tau \pi^- \pi^0 \bar{\mathrm{K}}^0$, and $\tau^- \to \nu_\tau \pi^- \mathrm{K}^0 \bar{\mathrm{K}}^0$ are allowed to vary in the fit. The other coefficients are fixed to the central values from the recently published measurements [12]: $\mathcal{B}(\tau^- \to \nu_\tau \mathrm{K}^- \mathrm{K}^0) = 0.0029 \pm 0.0012$ and $\mathcal{B}(\tau^- \to \nu_\tau \mathrm{K}^- \pi^0 \mathrm{K}^0) = 0.0005 \pm 0.0005$.

In order to increase the separation power between the channels, the coefficients of the linear combination are fit to a 10-bin histogram of the $\pi^0$ energy for the $\tau^- \to \nu_\tau \pi^- \pi^0 \bar{\mathrm{K}}^0$ sample. A $5 \times 3$ binned histogram of total decay energy versus invariant mass of the observed $\tau$ decay products is used for the $\tau^- \to \nu_\tau \pi^- \bar{\mathrm{K}}^0$ and $\tau^- \to \nu_\tau \pi^- \mathrm{K}^0 \bar{\mathrm{K}}^0$ samples. We use a binned maximum likelihood function which accounts for the finite statistics both in the data and in the Monte Carlo.

The spectrum used for the fit of the $\tau^- \to \nu_\tau \pi^- \pi^0 \bar{\mathrm{K}}^0$ sample is shown in Figure 4a together with the best fit Monte Carlo distributions. The total energy and invariant mass distributions

[3] In the $\mathrm{K}^- \mathrm{K}^0$ final state the energy is on average divided equally between the charged and neutral kaons, leading to small values of the ratio $\Delta E_{\mathrm{HC}}/\sqrt{P_\pi}$. In the case of the $\pi^- \bar{\mathrm{K}}^0$ final state, the (heavy) neutral kaon has more energy in the laboratory frame than the (light) charged pion, leading to large values of $\Delta E_{\mathrm{HC}}/\sqrt{P_\pi}$.

| | $\pi^-\bar{K}^0$ sample | $\pi^-\pi^0\bar{K}^0$ sample | $\pi^-K^0\bar{K}^0$ sample | Total |
|---|---|---|---|---|
| Data | 114 | 41 | 92 | 247 |
| $\tau^- \to \nu_\tau\pi^-\bar{K}^0$ | 71.9 | 2.4 | 37.7 | 112.0 |
| $\tau^- \to \nu_\tau K^-K^0$ | 10.0 | 0.1 | 3.8 | 13.9 |
| $\tau^- \to \nu_\tau\pi^-\pi^0\bar{K}^0$ | 3.5 | 20.3 | 9.3 | 33.1 |
| $\tau^- \to \nu_\tau K^-\pi^0K^0$ | 0.4 | 0.3 | 1.0 | 1.7 |
| $\tau^- \to \nu_\tau\pi^-K^0\bar{K}^0$ | 18.9 | 4.9 | 32.0 | 55.8 |
| Background | 11.8 | 7.5 | 8.4 | 27.7 |
| MC total | 116.5 | 35.5 | 82.2 | 244.2 |

Table 1: The numbers of decays detected in the three subsamples along with the best fit Monte Carlo expectations. For the $\tau^- \to \nu_\tau K^-K^0$ and $\tau^- \to \nu_\tau K^-\pi^0K^0$ channels, the numbers of expected decays correspond to the branching fractions measured in reference 12.

for the $\tau^- \to \nu_\tau\pi^-K^0\bar{K}^0$ and $\tau^- \to \nu_\tau\pi^-\bar{K}^0$ samples are shown in Figures 4b and 4c respectively together with the best fit Monte Carlo distributions.

The number of decays expected from the different channels is shown in Table 1 together with the corresponding number of data decays. The numbers of data decays in each channel from the fit are:

$$\begin{aligned}
N(\tau^- \to \nu_\tau\pi^-\bar{K}^0) &= 112.0 \pm 17.7 \\
N(\tau^- \to \nu_\tau\pi^-\pi^0\bar{K}^0) &= 33.1 \pm 9.7 \\
N(\tau^- \to \nu_\tau\pi^-K^0\bar{K}^0) &= 55.8 \pm 21.4
\end{aligned}$$

and the correlation coefficients between the fitted channels are

$$\begin{aligned}
\rho(\pi^-\bar{K}^0, \pi^-\pi^0\bar{K}^0) &= 0.01 \\
\rho(\pi^-\bar{K}^0, \pi^-K^0\bar{K}^0) &= 0.68 \\
\rho(\pi^-\pi^0\bar{K}^0, \pi^-K^0\bar{K}^0) &= 0.36 \ .
\end{aligned}$$

The large correlation coefficient between $N(\tau^- \to \nu_\tau\pi^-\bar{K}^0)$ and $N(\tau^- \to \nu_\tau\pi^-K^0\bar{K}^0)$ results in an increase of the statistical errors for the corresponding branching fractions. If we fix $N(\tau^- \to \nu_\tau\pi^-K^0\bar{K}^0)$ in the fit, the corresponding error for $N(\tau^- \to \nu_\tau\pi^-\bar{K}^0)$ is significantly reduced: $N(\tau^- \to \nu_\tau\pi^-\bar{K}^0) = 112.0 \pm 12.8$. Therefore, it is important to account for this correlation.

# Systematic Uncertainties

The dominant systematic errors in the measurement arise from the uncertainties in the absolute energy calibration and detector resolution functions, the background estimation, and theoretical uncertainties.

The calibration uncertainties affect both the selection efficiency and the shape of the final distributions used for the fit. The accuracy of the ECAL energy scale for electrons and photons is estimated to be 1% at 1 GeV from the measurement of the position of the $\pi^0$ mass peak and 0.1% at 45 GeV from a study of $Z \to e^+e^-(\gamma)$ events. The momentum scale of the central tracker is verified to 1% accuracy from 1 to 45 GeV using low energy electrons as well as muons from $\tau$ and Z decays. The absolute energy scales of the ECAL and HCAL for hadrons

| Source | | $\Delta N_{\pi^-\bar{K}^0}$ | $\Delta N_{\pi^-\pi^0\bar{K}^0}$ | $\Delta N_{\pi^-K^0\bar{K}^0}$ |
|---|---|---|---|---|
| | HCAL | 3.5 | 0.9 | 4.3 |
| Calibration | ECAL | 1.0 | 1.6 | 2.5 |
| | TEC | 1.0 | 0.8 | 0.6 |
| | $\pi^0$ | 2.0 | 0.8 | 0.6 |
| Background | $\pi^\pm/K^\pm$ | 1.5 | 0.5 | 0.6 |
| | $\Delta N_{K^-K^0}$ | 3.4 | 0.2 | 2.4 |
| | $\Delta N_{K^-\pi^0K^0}$ | 0.2 | 0.8 | 0.9 |
| Theory | matrix element | 3.9 | 1.2 | 4.0 |
| | $CP(K^0\bar{K}^0)$ | - | - | 2.7 |
| Total | $\Delta N^{syst}$ | 6.9 | 2.6 | 7.4 |

Table 2: Summary of the systematic uncertainties in the numbers of fitted decays.

are each known to 1.5% in the central region from the position of the $\rho$ mass peak. The corresponding uncertainties in the number of signal decays propagated through the selection and fitting procedures are listed in Table 2.

The resolution function of the HCAL is verified using test beam data and $\tau^- \to \rho^-\nu_\tau$ decays. The spectra of the ratio $\Delta E_{\rm HC}/\sqrt{P_\pi}$, as measured in the test beam for single pions of different energies, are compared with the Monte Carlo expectations in Figure 5. No discrepancy between data and Monte Carlo is observed within the achieved statistical errors, limiting possible uncertainty of the non-$K^0$ background to $\pm 2.1$ decays. The uncertainty in the number of decays with $K^0$'s due to inefficiency of the HCAL is estimated to be 1% of the number of fitted decays from a study of $Z \to \mu^+\mu^-(\gamma)$ events.

The systematic error due to the uncertainty in the rate of the decays $\tau^- \to \nu_\tau K^- K^0$ and $\tau^- \to \nu_\tau K^-\pi^0 K^0$ is estimated by varying their branching fractions according to the uncertainties quoted in reference 12. Uncertainties in the number of $\pi^0$'s from $\tau^- \to \rho^-\nu_\tau$ and $\tau^- \to a_1^-\nu_\tau$ decays leaking to the HCAL are estimated using a sample enriched with $\pi^0$'s with abnormally high energy deposition in the first three layers of the HCAL (seen as a peak at $E_{\rm 3L}/E_{\rm HC} \approx 1$ in Figure 1b). This uncertainty is estimated to be 20% of the number of $\tau^- \to \rho^-\nu_\tau$ and $\tau^- \to a_1^-\nu_\tau$ decays predicted by Monte Carlo simulation.

The theoretical error due to the uncertainty in the matrix element for the $\tau$ decays into three particles with one or two kaons arises from the non-uniformity of the selection efficiency over the phase space. In the Monte Carlo program [8] used to simulate $\tau$ decays, assumptions are made about the chiral structure of the weak hadronic current and the resonant structure of these decays. By varying these assumptions, we estimate the possible change of the efficiencies to be of the order 10%, depending slightly on the decay channel; the exact numbers are listed in Table 2. Another source of systematic error is the uncertainty in the CP phase of the $K^0\bar{K}^0$ system in the decay $\tau^- \to \nu_\tau\pi^- K^0\bar{K}^0$. The systematic error is assigned according to the difference in the fit results assuming that the $K^0\bar{K}^0$ sample consists of only CP-odd or only CP-even components. In the final fit, used to derive the branching fractions, the following proportion is assumed $K_L K_L : K_S K_S : K_S K_L = 0.25 : 0.25 : 0.5$.

Table 2 summarizes the study of the systematic errors for the numbers of fitted decays. When combining the systematic errors of a given channel, all sources are assumed to be independent.

## Discussion and Conclusions

From the fit results presented in Table 1, the selection efficiencies, and the total number of observed $\tau$ decays, we extract the following branching fractions:

$$\begin{aligned}\mathcal{B}(\tau^- \to \nu_\tau \pi^- \bar{\mathrm{K}}^0) &= 0.0095 \pm 0.0015(\mathrm{stat}) \pm 0.0006(\mathrm{syst}) \\ \mathcal{B}(\tau^- \to \nu_\tau \pi^- \pi^0 \bar{\mathrm{K}}^0) &= 0.0041 \pm 0.0012(\mathrm{stat}) \pm 0.0003(\mathrm{syst}) \\ \mathcal{B}(\tau^- \to \nu_\tau \pi^- \mathrm{K}^0 \bar{\mathrm{K}}^0) &= 0.0031 \pm 0.0012(\mathrm{stat}) \pm 0.0004(\mathrm{syst}).\end{aligned}$$

These results are consistent with other recent measurements [12–15] and comparable in accuracy.

Despite the absence of explicit identification of the final state charged hadron, these measurements are largely independent of the assumed branching fractions for $\tau^- \to \nu_\tau \mathrm{K}^- \mathrm{K}^0$ and $\tau^- \to \nu_\tau \mathrm{K}^- \pi^0 \mathrm{K}^0$. This is due to the fact that the selection efficiencies for these modes are significantly lower than the corresponding efficiencies for modes with charged pions, $\tau^- \to \nu_\tau \pi^- \bar{\mathrm{K}}^0$ and $\tau^- \to \nu_\tau \pi^- \pi^0 \bar{\mathrm{K}}^0$, as a result of the different kinematics of these decays.

The invariant mass spectrum of the $\pi^- \bar{\mathrm{K}}^0$ system agrees with the model that this final state comes only from $\tau^- \to \nu_\tau \mathrm{K}^{*-} \to \nu_\tau \pi^- \bar{\mathrm{K}}^0$. Assuming no other contributions to this final state, we extract

$$\mathcal{B}(\tau^- \to \nu_\tau \mathrm{K}^{*-}) = 0.0142 \pm 0.0022(\mathrm{stat}) \pm 0.009(\mathrm{syst}).$$

We have also considered the production of the $\pi^- \bar{\mathrm{K}}^0$ final state from higher mass resonances or nonresonant $\tau^-$ decays. Including these modes in the fit of our data, the following limits are derived:

$$\begin{aligned}\mathcal{B}(\tau^- \to \nu_\tau \pi^- \bar{\mathrm{K}}^0)_{\mathrm{nonresonant}} &< 0.0017 \quad \text{at 95\% CL;} \\ \mathcal{B}(\tau^- \to \nu_\tau \pi^- \bar{\mathrm{K}}^0)_{\mathrm{K}^{*-}(1430)} &< 0.0011 \quad \text{at 95\% CL.}\end{aligned}$$

The latter does not depend on the assumption of the spin of the $\mathrm{K}^{*-}(1430)$ resonance.

We have studied the resonant structure of the hadronic current in the $\tau^- \to \nu_\tau \pi^- \pi^0 \bar{\mathrm{K}}^0$ decay (Figure 6). The $\rho^-$ peak in the $\pi^- \pi^0$ invariant mass distribution is well reproduced by the Monte Carlo model [8] as shown in Figure 6a. However, Figure 6b and Figure 6c indicate a possible enhancement of the decays $\tau^- \to \nu_\tau \mathrm{K}_1^{*-} \to \nu_\tau \mathrm{K}^* \pi \to \nu_\tau \pi^- \pi^0 \bar{\mathrm{K}}^0$ in the data.

Our measurement of the branching fraction $\mathcal{B}(\tau^- \to \nu_\tau \pi^- \mathrm{K}^0 \bar{\mathrm{K}}^0)$ is insensitive to the theoretical assumptions on the matrix element and the CP phase of the $\mathrm{K}^0 \bar{\mathrm{K}}^0$ system. It is consistent within the achieved accuracy with measurements of the similar decay $\tau^- \to \nu_\tau \pi^- \mathrm{K}^- \mathrm{K}^+$ [13,15].

## Acknowledgments

We wish to express our gratitude to the CERN accelerator divisions for the excellent performance of the LEP machine. We acknowledge the efforts of all engineers and technicians who have participated in the construction and maintenance of this experiment.

## The L3 Collaboration:

M.Acciarri,[26] A.Adam,[43] O.Adriani,[16] M.Aguilar-Benitez,[25] S.Ahlen,[10] B.Alpat,[33] J.Alcaraz,[25] J.Allaby,[17] A.Aloisio,[28] G.Alverson,[11] M.G.Alviggi,[28] G.Ambrosi,[33] Q.An,[18] H.Anderhub,[46] V.P.Andreev,[37] T.Angelescu,[12] D.Antreasyan,[8] A.Arefiev,[27] T.Azemoon,[3] T.Aziz,[9] P.V.K.S.Baba,[18] P.Bagnaia,[36,17] L.Baksay,[42] R.C.Ball,[3] S.Banerjee,[9] K.Banicz,[43] R.Barillère,[17] L.Barone,[36] P.Bartalini,[33] A.Baschirotto,[26] M.Basile,[8] R.Battiston,[33] A.Bay,[22] F.Becattini,[16] U.Becker,[15] F.Behner,[46] Gy.L.Bencze,[13] J.Berdugo,[25] P.Berges,[15] B.Bertucci,[17] B.L.Betev,[46] M.Biasini,[33] A.Biland,[46] G.M.Bilei[33] R.Bizzarri,[36] J.J.Blaising,[17] G.J.Bobbink,[2] R.Bock,[1] A.Böhm,[1] B.Borgia,[36] A.Boucham,[4] D.Bourilkov,[46] M.Bourquin,[19] D.Boutigny,[4] B.Bouwens,[2] E.Brambilla,[15] J.G.Branson,[38] V.Brigljevic,[46] I.C.Brock,[34] A.Bujak,[43] J.D.Burger,[15] W.J.Burger,[19] C.Burgos,[25] J.Busenitz,[42] A.Buytenhuijs,[30] X.D.Cai,[18] M.Capell,[15] G.Cara Romeo,[8] M.Caria,[33] G.Carlino,[28] A.M.Cartacci,[16] J.Casaus,[25] G.Castellini,[16] R.Castello,[26] N.Cavallo,[28] C.Cecchi,[19] M.Cerrada,[25] F.Cesaroni,[36] M.Chamizo,[25] A.Chan,[48] Y.H.Chang,[48] U.K.Chaturvedi,[18] M.Chemarin,[24] A.Chen,[48] C.Chen,[6] G.Chen,[6] G.M.Chen,[6] H.F.Chen,[20] H.S.Chen,[6] M.Chen,[15] G.Chiefari,[28] C.Y.Chien,[5] M.T.Choi,[41] L.Cifarelli,[8] F.Cindolo,[8] C.Civinini,[16] I.Clare,[15] R.Clare,[15] T.E.Coan,[23] H.O.Cohn,[31] G.Coignet,[4] N.Colino,[17] V.Commichau,[1] S.Costantini,[36] F.Cotorobai,[12] B.de la Cruz,[25] X.T.Cui,[18] X.Y.Cui,[18] T.S.Dai,[15] R.D'Alessandro,[16] R.de Asmundis,[28] H.De Boeck,[30] A.Degré,[4] K.Deiters,[44] E.Dénes,[13] P.Denes,[35] F.DeNotaristefani,[36] D.DiBitonto,[42] M.Diemoz,[36] C.Dionisi,[36] M.Dittmar,[46] A.Dominguez,[38] A.Doria,[28] I.Dorne,[4] M.T.Dova,[18,♯] E.Drago,[28] D.Duchesneau,[17] P.Duinker,[2] I.Duran,[39] S.Dutta,[9] S.Easo,[33] Yu.Efremenko,[31] H.El Mamouni,[24] A.Engler,[34] F.J.Eppling,[15] F.C.Erné,[2] J.P.Ernenwein,[24] P.Extermann,[19] R.Fabbretti,[44] M.Fabre,[44] R.Faccini,[36] S.Falciano,[36] A.Favara,[16] J.Fay,[24] M.Felcini,[46] T.Ferguson,[34] D.Fernandez,[25] G.Fernandez,[25] F.Ferroni,[36] H.Fesefeldt,[1] E.Fiandrini,[33] J.H.Field,[19] F.Filthaut,[34] P.H.Fisher,[15] G.Forconi,[15] L.Fredj,[19] K.Freudenreich,[46] M.Gailloud,[22] Yu.Galaktionov,[27,15] S.N.Ganguli,[9] P.Garcia-Abia,[25] S.S.Gau,[11] S.Gentile,[36] J.Gerald,[5] N.Gheordanescu,[12] S.Giagu,[36] S.Goldfarb,[22] J.Goldstein,[10] Z.F.Gong,[20] E.Gonzalez,[25] A.Gougas,[5] D.Goujon,[19] G.Gratta,[32] M.W.Gruenewald,[7] C.Gu,[18] M.Guanziroli,[18] V.K.Gupta,[35] A.Gurtu,[9] H.R.Gustafson,[3] L.J.Gutay,[43] B.Hartmann,[1] A.Hasan,[29] J.T.He,[6] T.Hebbeker,[7] A.Hervé,[17] K.Hilgers,[1] W.C.van Hoek,[30] H.Hofer,[46] H.Hoorani,[19] S.R.Hou,[48] G.Hu,[18] M.M.Ilyas,[18] V.Innocente,[17] H.Janssen,[4] B.N.Jin,[6] L.W.Jones,[3] P.de Jong,[15] I.Josa-Mutuberria,[25] A.Kasser,[22] R.A.Khan,[18] Yu.Kamyshkov,[31] P.Kapinos,[45] J.S.Kapustinsky,[23] Y.Karyotakis,[4] M.Kaur,[18] S.Khokhar,[18] M.N.Kienzle-Focacci,[19] D.Kim,[5] J.K.Kim,[41] S.C.Kim,[41] Y.G.Kim,[41] W.W.Kinnison,[23] A.Kirkby,[32] D.Kirkby,[32] J.Kirkby,[17] S.Kirsch,[45] W.Kittel,[30] A.Klimentov,[15,27] A.C.König,[30] E.Koffeman,[2] O.Kornadt,[1] V.Koutsenko,[15,27] A.Koulbardis,[37] R.W.Kraemer,[34] T.Kramer,[15] W.Krenz,[1] H.Kuijten,[30] A.Kunin,[15,27] P.Ladron de Guevara,[25] G.Landi,[16] C.Lapoint,[15] K.Lassila-Perini,[46] P.Laurikainen,[21] M.Lebeau,[17] A.Lebedev,[15] P.Lebrun,[24] P.Lecomte,[46] J.Lecoq,[4] P.Lecoq,[17] P.Le Coultre,[46] J.S.Lee,[41] K.Y.Lee,[41] C.Leggett,[3] J.M.Le Goff,[17] R.Leiste,[45] M.Lenti,[16] E.Leonardi,[36] P.Levtchenko,[37] C.Li,[20,18] E.Lieb,[45] W.T.Lin,[48] F.L.Linde,[2] B.Lindemann,[1] L.Lista,[28] Y.Liu,[18] Z.A.Liu,[6] W.Lohmann,[45] E.Longo,[36] W.Lu,[32] Y.S.Lu,[6] K.Lübelsmeyer,[1] C.Luci,[36] D.Luckey,[15] L.Ludovici,[36] L.Luminari,[36] W.Lustermann,[44] W.G.Ma,[20] A.Macchiolo,[16] M.Maity,[9] L.Malgeri,[36] R.Malik,[18] A.Malinin,[27] C.Maña,[25] S.Mangla,[9] M.Maolinbay,[46] P.Marchesini,[46] A.Marin,[10] J.P.Martin,[24] F.Marzano,[36] G.G.G.Massaro,[2] K.Mazumdar,[9] D.McNally,[17] S.Mele,[28] M.Merk,[34] L.Merola,[28] M.Meschini,[16] W.J.Metzger,[30] Y.Mi,[22] A.Mihul,[12] A.J.W.van Mil,[30] Y.Mir,[18] G.Mirabelli,[36] J.Mnich,[17] M.Möller,[1] V.Monaco,[36] B.Monteleoni,[16] R.Moore,[3] R.Morand,[4] S.Morganti,[36] N.E.Moulai,[18] R.Mount,[32] S.Müller,[1] E.Nagy,[13] S.Nahn,[15] M.Napolitano,[28] F.Nessi-Tedaldi,[46] H.Newman,[32] M.A.Niaz,[18] A.Nippe,[1] H.Nowak,[45] G.Organtini,[36] R.Ostonen,[21] D.Pandoulas,[1] S.Paoletti,[36] P.Paolucci,[28] G.Pascale,[36] G.Passaleva,[16] S.Patricelli,[28] T.Paul,[33] M.Pauluzzi,[33] C.Paus,[1] F.Pauss,[46] Y.J.Pei,[1] S.Pensotti,[26] D.Perret-Gallix,[4] A.Pevsner,[5] D.Piccolo,[28] M.Pieri,[16] J.C.Pinto,[34] P.A.Piroué,[35] E.Pistolesi,[16] V.Plyaskin,[27] M.Pohl,[46] V.Pojidaev,[27,16] H.Postema,[15] N.Produit,[19] K.N.Qureshi,[18] R.Raghavan,[9] G.Rahal-Callot,[46] P.G.Rancoita,[26] M.Rattaggi,[26] G.Raven,[2] P.Razis,[29] K.Read,[31] M.Redaelli,[26] D.Ren,[46] Z.Ren,[18] M.Rescigno,[36] S.Reucroft,[11] A.Ricker,[1] S.Riemann,[45] B.C.Riemers,[43] K.Riles,[3] O.Rind,[3] H.A.Rizvi,[18] S.Ro,[41] A.Robohm,[46] J.Rodin,[15] F.J.Rodriguez,[25] B.P.Roe,[3] M.Röhner,[1] S.Röhner,[1] L.Romero,[25] S.Rosier-Lees,[4] Ph.Rosselet,[22] W.van Rossum,[2] S.Roth,[1] J.A.Rubio,[17] H.Rykaczewski,[46] J.Salicio,[17] J.M.Salicio,[25] E.Sanchez,[25] A.Santocchia,[33] M.E.Sarakinos,[21] S.Sarkar,[9] G.Sartorelli,[18] M.Sassowsky,[1] G.Sauvage,[4] C.Schäfer,[1] V.Schegelsky,[37] D.Schmitz,[1] P.Schmitz,[1] M.Schneegans,[4] B.Schoeneich,[45] N.Scholz,[46] H.Schopper,[47] D.J.Schotanus,[30] R.Schulte,[1] K.Schultze,[1] J.Schwenke,[1] G.Schwering,[1] C.Sciacca,[28] R.Sehgal,[18] P.G.Seiler,[44] J.C.Sens,[48] L.Servoli,[33] S.Shevchenko,[32] N.Shivarov,[40] V.Shoutko,[27] J.Shukla,[23] E.Shumilov,[27] D.Son,[41] A.Sopczak,[17] V.Soulimov,[28] B.Smith,[15] T.Spickermann,[1] P.Spillantini,[16] M.Steuer,[15] D.P.Stickland,[35] F.Sticozzi,[15] H.Stone,[35] B.Stoyanov,[40] K.Strauch,[14] K.Sudhakar,[9] G.Sultanov,[18] L.Z.Sun,[20,18] G.F.Susinno,[19] H.Suter,[46] J.D.Swain,[18] A.A.Syed,[30] X.W.Tang,[6] L.Taylor,[11] R.Timellini,[8] Samuel C.C.Ting,[15] S.M.Ting,[15] O.Toker,[33] M.Tonutti,[1] S.C.Tonwar,[9] J.Tóth,[13] A.Tsaregorodtsev,[37] G.Tsipolitis,[34] C.Tully,[35] H.Tuchscherer,[42] J.Ulbricht,[46] L.Urbán,[13] U.Uwer,[1] E.Valente,[36] R.T.Van de Walle,[30] I.Vetlitsky,[27] G.Viertel,[46] P.Vikas,[18] U.Vikas,[18] M.Vivargent,[4] R.Voelkert,[45] H.Vogel,[34] H.Vogt,[45] I.Vorobiev,[27] A.A.Vorobyov,[37] An.A.Vorobyov,[37] L.Vuilleumier,[22] M.Wadhwa,[25] W.Wallraff,[1] J.C.Wang,[15] X.L.Wang,[20] Y.F.Wang,[15] Z.M.Wang,[18,20] A.Weber,[1] R.Weill,[22] C.Willmott,[25] F.Wittgenstein,[17] S.X.Wu,[18] S.Wynhoff,[1] J.Xu,[10] Z.Z.Xu,[20] B.Z.Yang,[20] C.G.Yang,[6] G.Yang,[18] X.Y.Yao,[6] C.H.Ye,[18] J.B.Ye,[20] Q.Ye,[18] S.C.Yeh,[48] J.M.You,[34] N.Yunus,[18] M.Yzerman,[2] C.Zaccardelli,[32] An.Zalite,[37] P.Zemp,[46] J.Y.Zeng,[6] M.Zeng,[18] Y.Zeng,[1] Z.Zhang,[6] Z.P.Zhang,[20,18] B.Zhou,[10] G.J.Zhou,[6] J.F.Zhou,[1] Y.Zhou,[3] G.Y.Zhu,[6] R.Y.Zhu,[32] A.Zichichi,[8,17,18] B.C.C.van der Zwaan.[2]

1 I. Physikalisches Institut, RWTH, D-52056 Aachen, FRG[§]
III. Physikalisches Institut, RWTH, D-52056 Aachen, FRG[§]
2 National Institute for High Energy Physics, NIKHEF, NL-1009 DB Amsterdam, The Netherlands
3 University of Michigan, Ann Arbor, MI 48109, USA
4 Laboratoire d'Annecy-le-Vieux de Physique des Particules, LAPP,IN2P3-CNRS, BP 110, F-74941 Annecy-le-Vieux CEDEX, France
5 Johns Hopkins University, Baltimore, MD 21218, USA
6 Institute of High Energy Physics, IHEP, 100039 Beijing, China
7 Humboldt University, D-10099 Berlin, FRG[§]
8 INFN-Sezione di Bologna, I-40126 Bologna, Italy
9 Tata Institute of Fundamental Research, Bombay 400 005, India
10 Boston University, Boston, MA 02215, USA
11 Northeastern University, Boston, MA 02115, USA
12 Institute of Atomic Physics and University of Bucharest, R-76900 Bucharest, Romania
13 Central Research Institute for Physics of the Hungarian Academy of Sciences, H-1525 Budapest 114, Hungary[‡]
14 Harvard University, Cambridge, MA 02139, USA
15 Massachusetts Institute of Technology, Cambridge, MA 02139, USA
16 INFN Sezione di Firenze and University of Florence, I-50125 Florence, Italy
17 European Laboratory for Particle Physics, CERN, CH-1211 Geneva 23, Switzerland
18 World Laboratory, FBLJA Project, CH-1211 Geneva 23, Switzerland
19 University of Geneva, CH-1211 Geneva 4, Switzerland
20 Chinese University of Science and Technology, USTC, Hefei, Anhui 230 029, China
21 SEFT, Research Institute for High Energy Physics, P.O. Box 9, SF-00014 Helsinki, Finland
22 University of Lausanne, CH-1015 Lausanne, Switzerland
23 Los Alamos National Laboratory, Los Alamos, NM 87544, USA
24 Institut de Physique Nucléaire de Lyon, IN2P3-CNRS,Université Claude Bernard, F-69622 Villeurbanne Cedex, France
25 Centro de Investigaciones Energeticas, Medioambientales y Tecnologicas, CIEMAT, E-28040 Madrid, Spain♭
26 INFN-Sezione di Milano, I-20133 Milan, Italy
27 Institute of Theoretical and Experimental Physics, ITEP, Moscow, Russia
28 INFN-Sezione di Napoli and University of Naples, I-80125 Naples, Italy
29 Department of Natural Sciences, University of Cyprus, Nicosia, Cyprus
30 University of Nymegen and NIKHEF, NL-6525 ED Nymegen, The Netherlands
31 Oak Ridge National Laboratory, Oak Ridge, TN 37831, USA
32 California Institute of Technology, Pasadena, CA 91125, USA
33 INFN-Sezione di Perugia and Universitá Degli Studi di Perugia, I-06100 Perugia, Italy
34 Carnegie Mellon University, Pittsburgh, PA 15213, USA
35 Princeton University, Princeton, NJ 08544, USA
36 INFN-Sezione di Roma and University of Rome, "La Sapienza", I-00185 Rome, Italy
37 Nuclear Physics Institute, St. Petersburg, Russia
38 University of California, San Diego, CA 92093, USA
39 Dept. de Fisica de Particulas Elementales, Univ. de Santiago, E-15706 Santiago de Compostela, Spain
40 Bulgarian Academy of Sciences, Central Laboratory of Mechatronics and Instrumentation, BU-1113 Sofia, Bulgaria
41 Center for High Energy Physics, Korea Advanced Inst. of Sciences and Technology, 305-701 Taejon, Republic of Korea
42 University of Alabama, Tuscaloosa, AL 35486, USA
43 Purdue University, West Lafayette, IN 47907, USA
44 Paul Scherrer Institut, PSI, CH-5232 Villigen, Switzerland
45 DESY-Institut für Hochenergiephysik, D-15738 Zeuthen, FRG
46 Eidgenössische Technische Hochschule, ETH Zürich, CH-8093 Zürich, Switzerland
47 University of Hamburg, D-22761 Hamburg, FRG
48 High Energy Physics Group, Taiwan, China
§ Supported by the German Bundesministerium für Bildung, Wissenschaft, Forschung und Technologie
‡ Supported by the Hungarian OTKA fund under contract number 2970.
♭ Supported also by the Comisión Interministerial de Ciencia y Technología
♯ Also supported by CONICET and Universidad Nacional de La Plata, CC 67, 1900 La Plata, Argentina

# References


[1] Particle Data Group, L. Montanet *et al.*, Review of Particle Properties, *Phys. Rev.* **D50** (1994) 1406.

[2] R. Decker *et al.*, *Phys. Rev.* **D50** (1994) 6863.

[3] E. Braaten *et al.*, *Int. J. Mod. Phys.* **A5** (1990) 2737.

[4] L3 Collaboration, B. Adeva *et al.*, *Nucl. Instr. and Meth.* **A289** (1990) 35;
O. Adriani *et al.*, *Nucl. Instr. and Meth.* **A302** (1991) 53;
K. Deiters *et al.*, *Nucl. Instr. and Meth.* **A323** (1992) 162;
J. A. Bakken, *Nucl. Instr. and Meth.* **A275** (1989) 81.

[5] A. Arefiev *et al.*, *Nucl. Instr. and Meth.* **A251** (1986) 258;
A. Arefiev *et al.*, *Nucl. Instr. and Meth.* **A285** (1989) 403.

[6] L3 Collaboration, O.Adriani *et al.*, *Phys. Lett.* **B294** (1992) 466;
L3 Collaboration, O.Acciarri *et al.*, *Phys. Lett.* **B341** (1994) 245.

[7] S. Jadach, B.F.L. Ward and Z. Wąs, *Comp. Phys. Comm.* **66** (1991) 276;
R. Kleiss *et al.*, in "Z Physics at LEP1", CERN Report CERN 89-08 (1989), Vol. 3, p. 1.

[8] S. Jadach *et al.*,, *Comp. Phys. Comm.* **76** (1994) 361;
S. Jadach, J.H. Kühn and Z. Wąs, *Comp. Phys. Comm.* **64** (1991) 275.

[9] R. Brun *et al.*, "GEANT 3", CERN DD/EE/84-1 (Revised), September 1987.

[10] H. Fesefeldt, RWTH Aachen Preprint PITHA 85/02 (1985).

[11] T. Sjöstrand and M. Bengtsson, *Comp. Phys. Comm.* **43** (1987) 367;
T. Sjöstrand *et al.*, in "Z Physics at LEP1", CERN Report CERN 89-08 (1989), Vol. 3, p. 143.

[12] ALEPH Collaboration, D. Buskulic *et al.*, *Phys. Lett.* **B332** (1994) 219.

[13] DELCO Collaboration, G.B. Mills *et al.*, *Phys. Rev. Lett.* **54** (1985) 624.

[14] OPAL Collaboration, R. Akers *et al.*, *Phys. Lett.* **B339** (1994) 278.

[15] TPC/2$\gamma$ Collaboration, D.A. Bauer *et al.*, *Phys. Rev.* **D50** (1994) 13.

# Figure Captions

Figure 1. (a) The spectrum of the ratio $\Delta E_{\mathrm{HC}}/\sqrt{P_\pi}$ for the preselected decays. The hatched area corresponds to the contribution of the $\tau^- \to \nu_\tau \pi^- \bar{\mathrm{K}}^0$, $\tau^- \to \nu_\tau \mathrm{K}^- \mathrm{K}^0$, $\tau^- \to \nu_\tau \pi^- \pi^0 \bar{\mathrm{K}}^0$, $\tau^- \to \nu_\tau \pi^- \pi^0 \bar{\mathrm{K}}^0$, $\tau^- \to \nu_\tau \mathrm{K}^- \pi^0 \mathrm{K}^0$ decay modes. (b) The spectrum of the fraction of the HCAL energy deposited in the first three layers. The cut on the ratio $\Delta E_{\mathrm{HC}}/\sqrt{P_\pi}$ is already applied. (c) The separation angle between the charged hadron and cluster in the HCAL. All other cuts are already applied. The arrows in (a)-(c) indicate the corresponding values of the applied cuts.

Figure 2. A $\tau^- \to \nu_\tau \pi^- \pi^0 \bar{\mathrm{K}}^0$ candidate decay. In the upper hemisphere, the 1.36 GeV/c charged track is well separated in space from the 12.0 GeV $\pi^0$ detected in the ECAL and the 12.6 GeV neutral hadron shower in the HCAL. The neutral hadron shower starts after 3 HCAL layers (about $0.7\lambda$).

Figure 3. A $\tau^- \to \nu_\tau \pi^- \mathrm{K}^0 \bar{\mathrm{K}}^0$ candidate decay. In the upper hemisphere, the 2.39 GeV/c charged track is separated in space from the 9.4 GeV cluster in the ECAL and the 33.6 GeV neutral hadron shower in the HCAL. The neutral hadron shower has two distinct local maxima: about 12 GeV in the front part of the HCAL and 20 GeV in the back part. The shower shape of the neutral energy cluster in the ECAL is inconsistent with being a $\pi^0$.

Figure 4. (a) The spectrum of the $\pi^0$ energy for the sample enriched with $\tau^- \to \nu_\tau \pi^- \pi^0 \bar{\mathrm{K}}^0$ decays. (b) The spectrum of the sum of energies of the observed $\tau$ decay products for the sample enriched with $\tau^- \to \nu_\tau \pi^- \mathrm{K}^0 \bar{\mathrm{K}}^0$ decays. (c) The invariant mass spectrum of the $\pi^- \bar{\mathrm{K}}^0$ system for the sample enriched with $\tau^- \to \nu_\tau \pi^- \bar{\mathrm{K}}^0$ decays.

Figure 5. The spectra of the ratio $\Delta E_{\mathrm{HC}}/\sqrt{P_\pi}$ for (a) 4 GeV and (b) 8 GeV single pions as measured in the test-beam (dots) and predicted by the Monte Carlo (solid histogram).

Figure 6. (a) The invariant mass spectrum of the $\pi^- \pi^0$ system for the sample enriched with $\tau^- \to \nu_\tau \pi^- \pi^0 \bar{\mathrm{K}}^0$ decays. (b) The invariant mass spectrum of the $\pi^- \bar{\mathrm{K}}^0$ system for the sample enriched with $\tau^- \to \nu_\tau \pi^- \pi^0 \bar{\mathrm{K}}^0$ decays. (c) The invariant mass spectrum of the $\pi^- \pi^0 \bar{\mathrm{K}}^0$ system for the sample enriched with $\tau^- \to \nu_\tau \pi^- \pi^0 \bar{\mathrm{K}}^0$ decays.

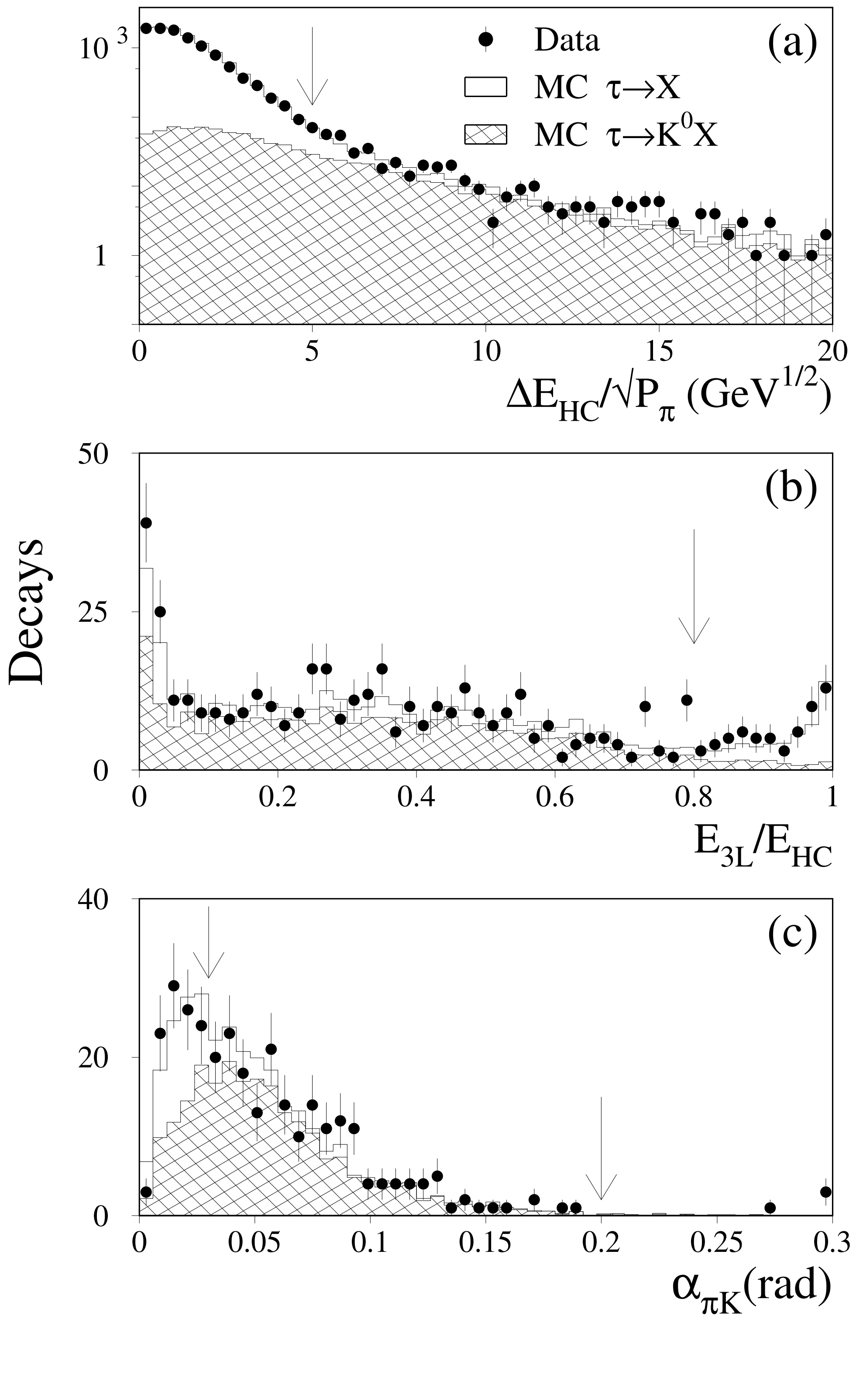


**Figure 1**

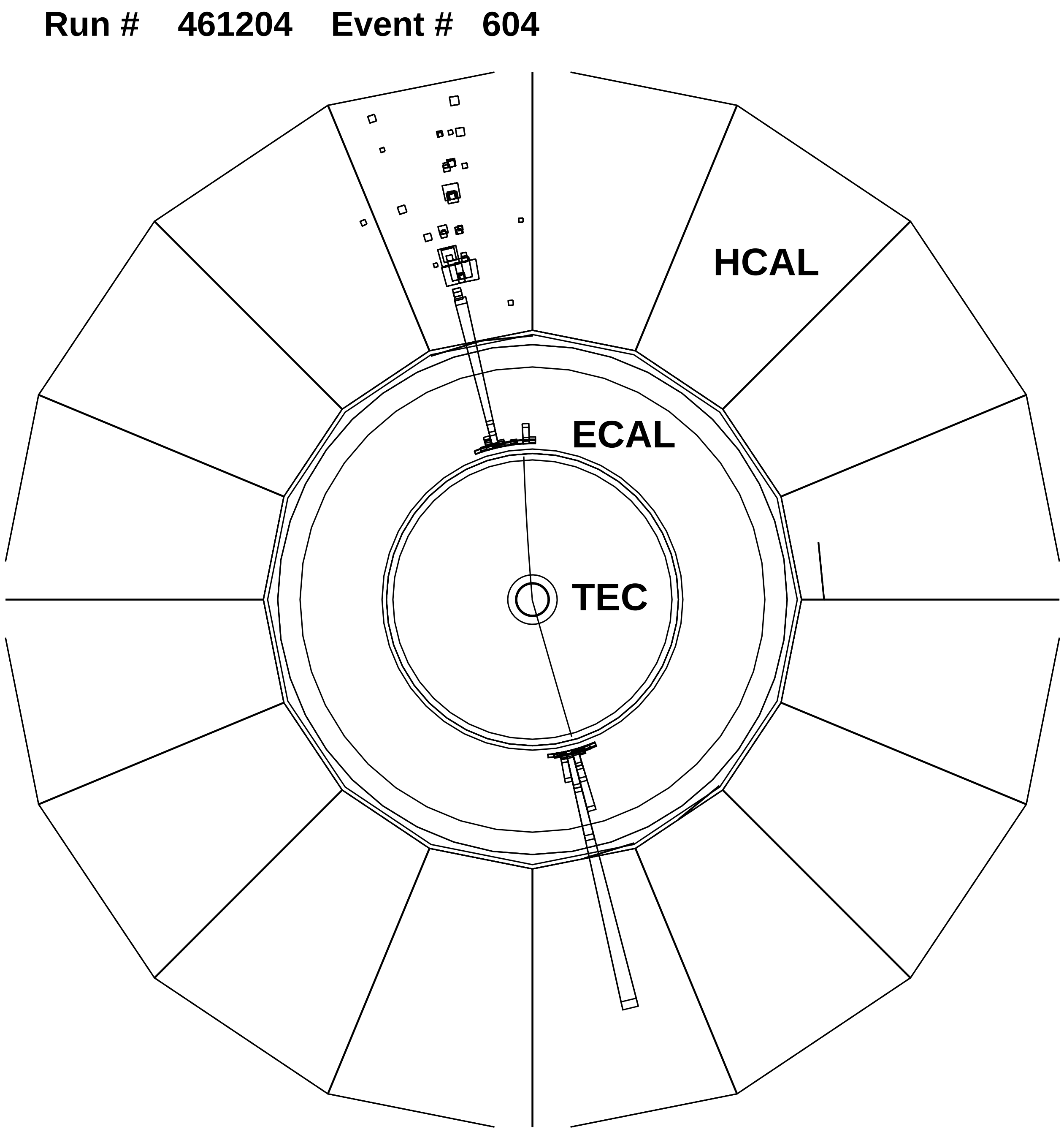


**Figure 2**

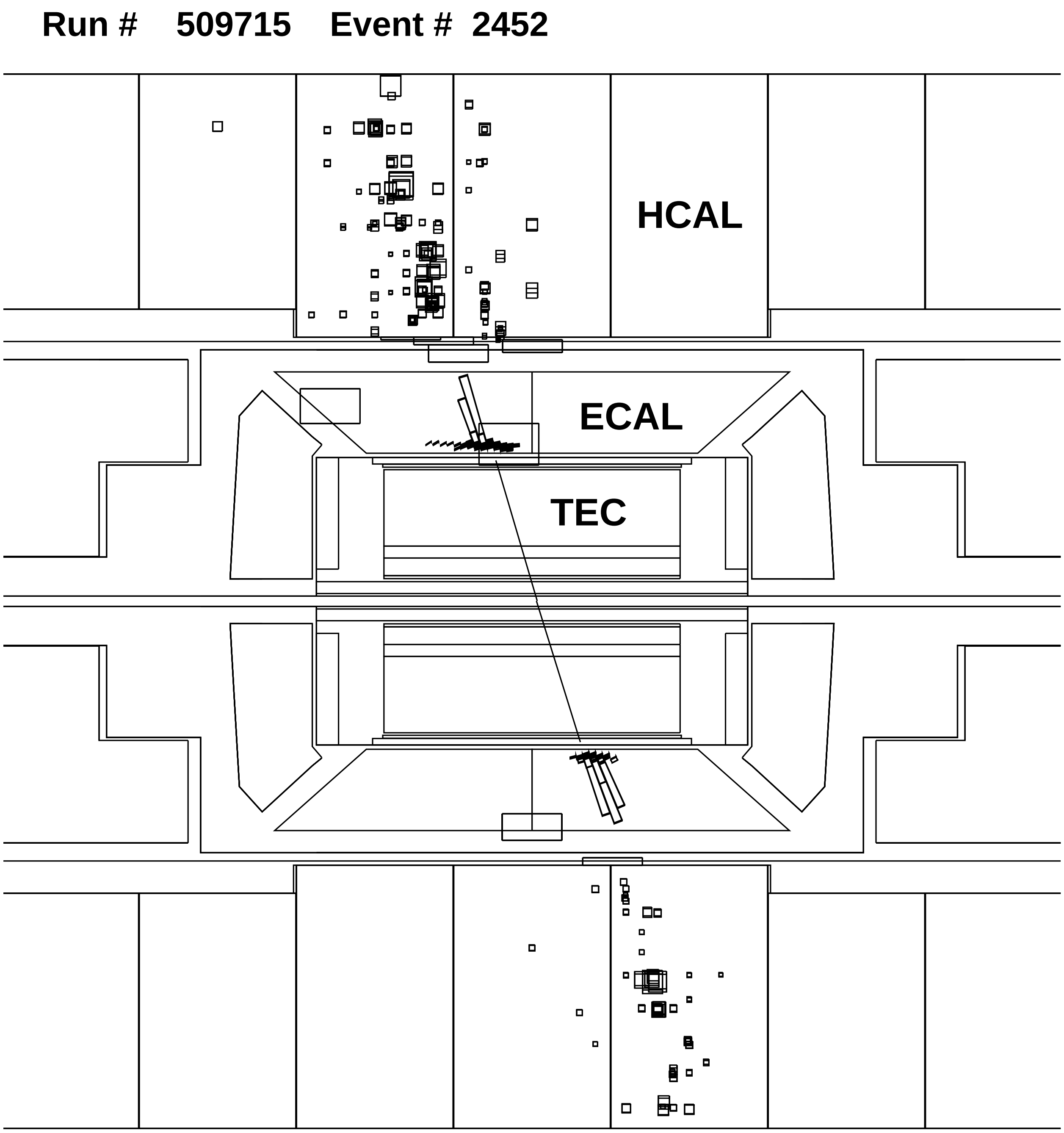


**Figure 3**

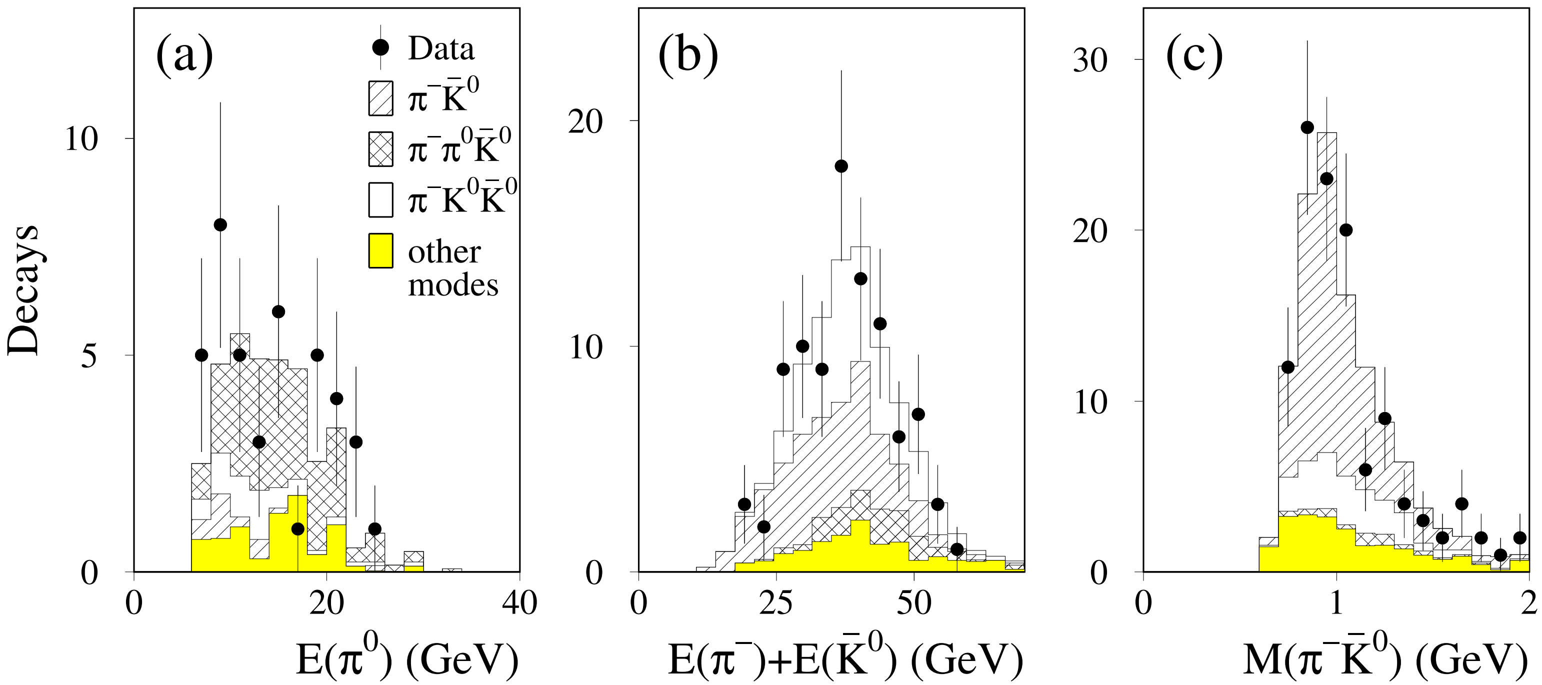

(a)
(b)
(c)
Data
$\pi^-\bar{K}^0$
$\pi^-\pi^0\bar{K}^0$
$\pi^-K^0\bar{K}^0$
other modes
Decays
$E(\pi^0)$ (GeV)
$E(\pi^-)+E(\bar{K}^0)$ (GeV)
$M(\pi^-\bar{K}^0)$ (GeV)


Figure 4

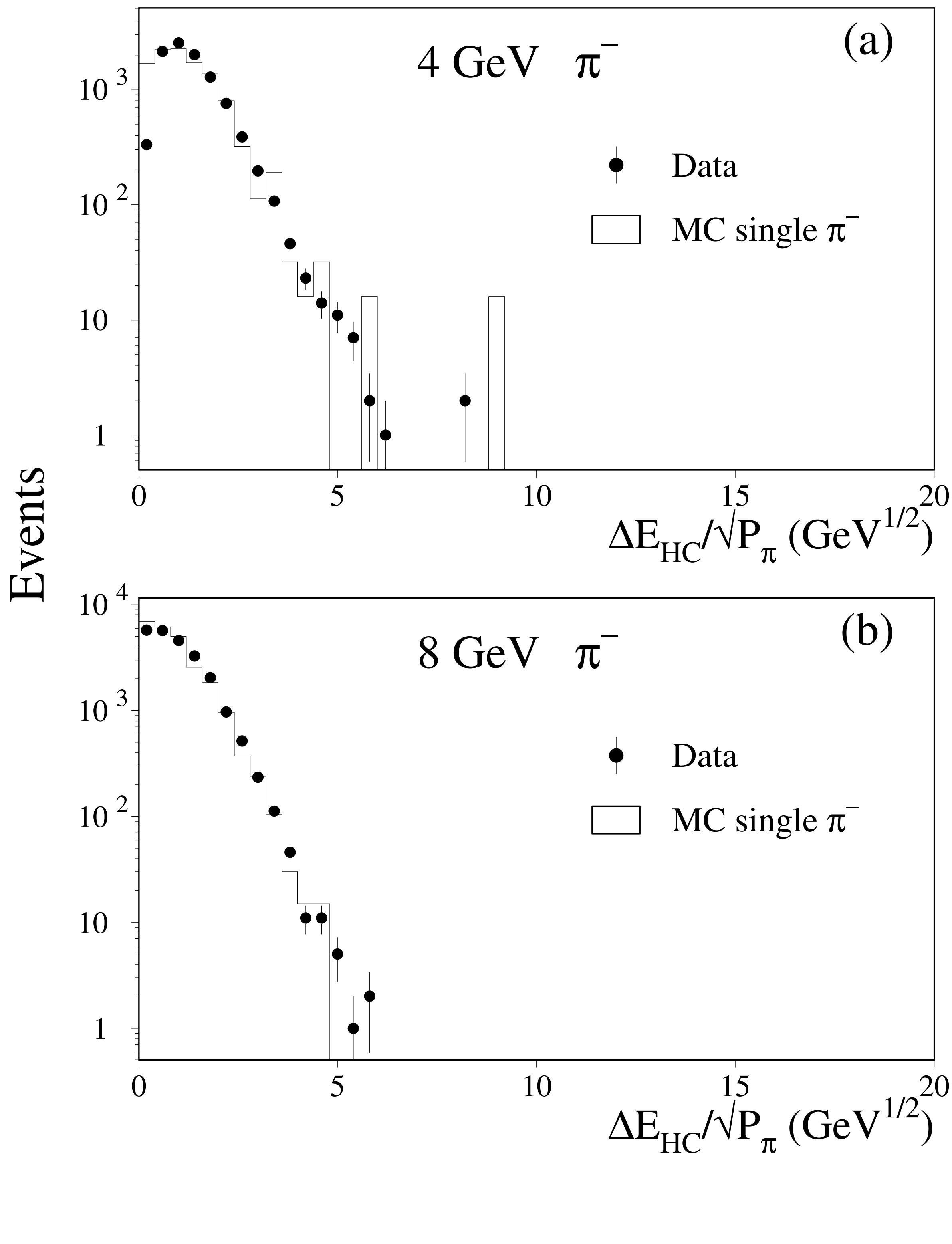
4 GeV $\pi^-$
(a)
Data
MC single $\pi^-$
8 GeV $\pi^-$
(b)
Events
$\Delta E_{HC}/\sqrt{P_\pi}$ (GeV$^{1/2}$)
$10^4$
$10^3$
$10^2$
10
1
0
5
10
15
20

**Figure 5**

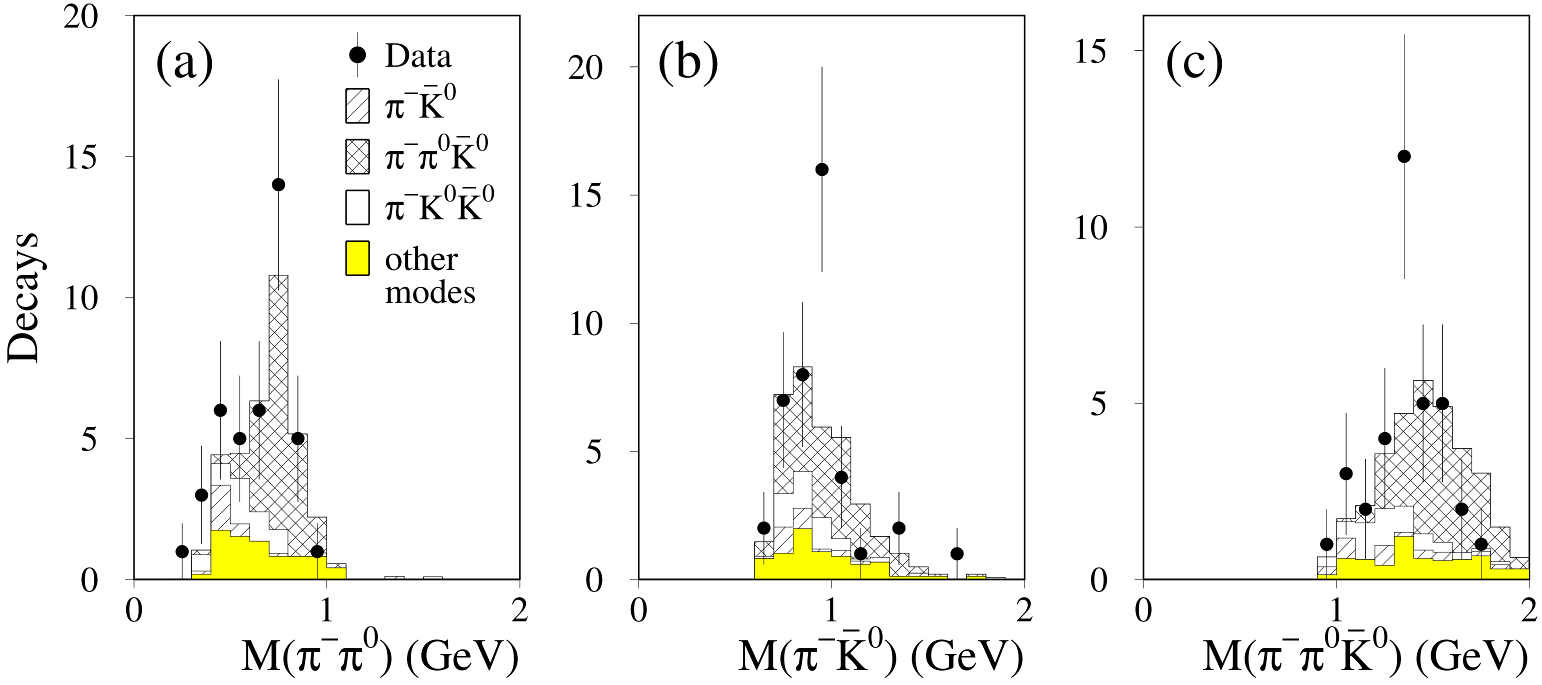
(a)
(b)
(c)
Data
$\pi^-\bar{K}^0$
$\pi^-\pi^0\bar{K}^0$
$\pi^-K^0\bar{K}^0$
other modes
Decays
$M(\pi^-\pi^0)$ (GeV)
$M(\pi^-\bar{K}^0)$ (GeV)
$M(\pi^-\pi^0\bar{K}^0)$ (GeV)

Figure 6